

Local and Global Contrast Adaptation in Retinal Ganglion Cells

Mona M. Garvert^{1,4} and Tim Gollisch^{1,2,3,*}

¹Visual Coding Group, Max Planck Institute of Neurobiology, 82152 Martinsried, Germany

²Department of Ophthalmology, University Medical Center Göttingen, 37073 Göttingen, Germany

³Bernstein Center for Computational Neuroscience Göttingen, 37073 Göttingen, Germany

⁴Present address: University College London, Wellcome Trust Centre for Neuroimaging, London WC1N 3BG, UK

*Correspondence: tim.gollisch@med.uni-goettingen.de

<http://dx.doi.org/10.1016/j.neuron.2012.12.030>

SUMMARY

Retinal ganglion cells react to changes in visual contrast by adjusting their sensitivity and temporal filtering characteristics. This contrast adaptation has primarily been studied under spatially homogeneous stimulation. Yet, ganglion cell receptive fields are often characterized by spatial subfields, providing a substrate for nonlinear spatial processing. This raises the question whether contrast adaptation follows a similar subfield structure or whether it occurs globally over the receptive field even for local stimulation. We therefore recorded ganglion cell activity in isolated salamander retinas while locally changing visual contrast. Ganglion cells showed primarily global adaptation characteristics, with notable exceptions in certain aspects of temporal filtering. Surprisingly, some changes in filtering were most pronounced for locations where contrast did not change. This seemingly paradoxical effect can be explained by a simple computational model, which emphasizes the importance of local nonlinearities in the retina and suggests a reevaluation of previously reported local contrast adaptation.

INTRODUCTION

Neurons have a limited dynamic range in their output, yet they have to encode stimuli under a wide variety of natural conditions. For many sensory systems, including visual (Maffei et al., 1973; Shapley and Victor, 1978; Movshon and Lennie, 1979), auditory (Kvale and Schreiner, 2004; Nagel and Doupe, 2006), and somatosensory (Garcia-Lazaro et al., 2007; Maravall et al., 2007) systems, it has been found that neurons cope with this challenge by adjusting their operating characteristics to the variance of encountered stimulus intensities. For the visual system, this begins in the retina, where ganglion cells show adaptation to visual contrast (Shapley and Victor, 1978; Smirnakis et al., 1997; Chander and Chichilnisky, 2001; Kim and Rieke, 2001; Baccus and Meister, 2002; Beaudoin et al., 2008) and pass on these effects to downstream brain areas (Solomon et al., 2004; Bonin

et al., 2005). Higher contrast leads to reduced sensitivity of retinal ganglion cells as well as altered temporal filtering characteristics, which manifest themselves in faster responses, shorter integration times, and a preference for higher temporal frequencies.

Little is known, however, about the spatial scope of these different contrast adaptation effects. Ganglion cells typically pool visual inputs over their receptive fields through an array of parallel bipolar cells with smaller receptive fields (Freed and Sterling, 1988; Kolb and Nelson, 1993; Ölüveczky et al., 2003; Schwartz et al., 2012). It has been shown that several types of ganglion cells perform this spatial integration by combining signals in a nonlinear way from small subfields within the receptive field, which endows the cells with specific functional properties (Ölüveczky et al., 2003; Münch et al., 2009; Gollisch and Meister, 2010; Azeredo da Silveira and Roska, 2011; Bölinger and Gollisch, 2012). This raises questions as to how the observed spatial nonlinearities affect the characteristic features of contrast adaptation, and whether contrast adaptation is also organized in a spatial subfield structure so that local subfields can undergo contrast adaptation independently. Alternatively, contrast adaptation could occur globally and always affect the entire receptive field of a ganglion cell.

Previous analyses have provided evidence for either possibility. Contrast adaptation has been attributed to synaptic inputs (Kim and Rieke, 2001; Manookin and Demb, 2006; Beaudoin et al., 2007) as well as to intrinsic mechanisms of ganglion cells (Kim and Rieke, 2001, 2003; Weick and Demb, 2011), thus providing substrates for adaptation both before and after spatial pooling. Furthermore, contrast adaptation effects were found to be independent of the spatial phase of an adapting grating stimulus (Shapley and Victor, 1978), and effects of increased contrast over the receptive field center were mimicked by peripheral stimulation (Shapley and Victor, 1979). This led to the hypothesis that the relevant contrast measure for inducing contrast adaptation is derived from an area as large as or larger than the ganglion cell's receptive field (Shapley and Victor, 1981). More recently, however, it was reported that different locations within a ganglion cell's receptive field could adapt independently, because switching the stimulation from one location to another briefly increased the firing rate, suggesting that the new location had not yet adapted (Brown and Masland, 2001).

In this work, we set out to directly investigate how visual contrast in subfields of a ganglion cell's receptive field affects

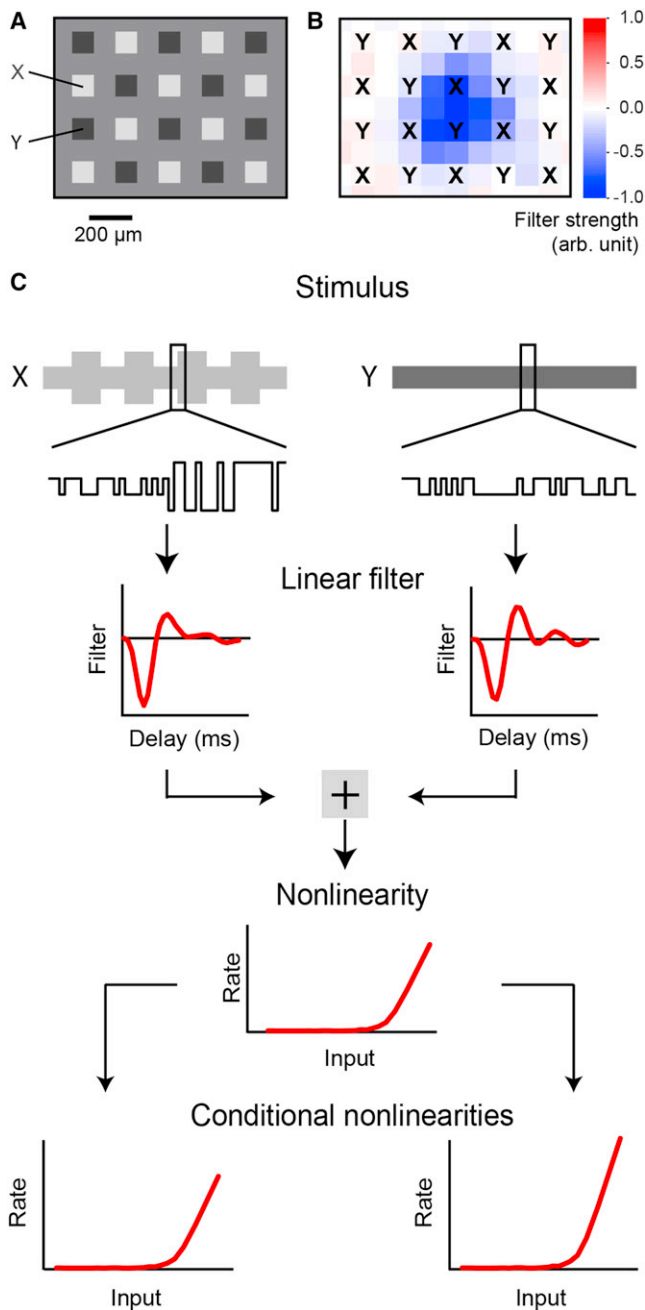


Figure 1. Stimulus and Model for Analyzing the Spatial Scale of Contrast Adaptation

(A) One frame of the stimulus used in the study. Here, all bright squares correspond to locations X and all dark squares correspond to locations Y, arranged in a regular layout on top of a gray background.

(B) Receptive field of a sample ganglion cell with respect to the layout of locations X and Y.

(C) LN model used to analyze stimulus processing separately at locations X and Y. At the top, the applied stimuli are shown schematically by the envelope of the white-noise sequences at both X and Y, indicating the changes in contrast level at locations X every 90 s, and by short traces of binary white noise (not to scale). These inputs are then filtered by a spatiotemporal filter, which can be represented by its two temporal components for X and Y, respectively. The final nonlinear transformation of the filtered signal can be

sensitivity and temporal filtering in other subfields. Based on extracellular recordings of spiking activity in isolated salamander retina, we show that global changes of sensitivity and filtering predominate, with local contrast providing only a minor contribution. Unexpectedly, however, certain local changes in filtering were most pronounced at locations where contrast did not change. Finally, we show that this seemingly paradoxical finding can be explained by a simple computational model. These findings shed new light on the spatial organization of contrast adaptation and how it is affected by local receptive field nonlinearities.

RESULTS

Visual Stimulus for Analyzing the Spatial Structure of Contrast Adaptation

Contrast adaptation in the retina is typically studied by stimulating the retina with a temporal flicker of light intensity, incorporating sudden changes in the magnitude of the flicker around the mean light level. The characteristic response features are then extracted by fitting the measured responses with a linear-nonlinear (LN) model for each applied contrast level (Chander and Chichilnisky, 2001; Kim and Rieke, 2001; Baccus and Meister, 2002; Zaghloul et al., 2005; Wark et al., 2007; Demb, 2008). To determine whether contrast adaptation can occur locally in subfields of the receptive field, we extended this standard stimulus paradigm by flickering light intensities independently at two distinct sets of spatial subfields, denoted as locations X and Y, respectively (Figure 1A). All locations X always displayed the same light intensity, chosen randomly every 30 ms from a binary distribution, whereas an independent random binary sequence of light intensities was shown at all locations Y. We projected this stimulus onto the photoreceptor layer of isolated salamander retinas and recorded ganglion cell spikes extracellularly with multielectrode arrays.

The subfield structure of nonlinear receptive fields is thought to arise from the convergence of bipolar cell signals (Demb et al., 1999, 2001), which have furthermore been suggested to mechanistically contribute to contrast adaptation (Kim and Rieke, 2001; Manookin and Demb, 2006; Beaudoin et al., 2007). We therefore chose the stimulus subfields to be squares measuring 90 μm on each side, which matches the receptive field size of typical bipolar cells in the salamander retina, for which measured diameters lie roughly in the range of 50–100 μm (Wu et al., 2000; Ölveczky et al., 2003; Baccus et al., 2008). The stimulus subfields were separated from each other by 90 μm of constant gray background light intensity, so we can assume that each bipolar cell was primarily driven by either stimulus component X or Y, but not both. Each ganglion cell's receptive field center typically covered a small number of individual subfields from each of the two stimulus components, X and Y (Figure 1B). This ensured that most ganglion cells were driven about equally well by stimuli occurring at X or Y. We then switched the contrast level at locations X every 90 s (Figure 1C) and asked whether or not these contrast changes

further analyzed through conditional nonlinearities for each spatial component by selecting stimulus segments for which the other spatial component yielded filter signals close to zero.

at X affected stimulus processing at locations Y where contrast stayed constant.

Analyzing neural responses in the framework of the LN model is an expedient way to extract measures of sensitivity and temporal filtering in the context of contrast adaptation, because it allows one to associate changes in response kinetics and sensitivity with parameter changes in the temporal filter and nonlinear transformation of this model. Therefore, we also based our analysis of the spatial scope of the different contrast adaptation effects on the LN model (Figure 1C). In the first stage of the model, the stimulus is passed through a linear spatiotemporal filter with two spatial components corresponding to X and Y, respectively. For plotting purposes and for capturing effects related to the individual spatial components, we can equivalently separate this spatiotemporal filter into its two spatial components and consider two purely temporal filters, one for each spatial component, with subsequent summation. The filters were determined from the data by a spike-triggered-average analysis and normalized to have the same total power for easier comparison of filter shapes.

In the second stage of the model, the output of the linear filter is transformed by a nonlinear function, resulting in the model's instantaneous firing rate. In order to separately analyze the sensitivity of the neuron to its inputs at locations X and Y, we further computed nonlinearities by using only such stimulus episodes where the filtered stimulus at the other locations (Y or X, respectively) yielded a value close to zero. These conditional nonlinearities (Figure 1C) capture how effective stimulation at each set of locations is by itself (Samengo and Gollisch, 2013). Extracting the filters and conditional nonlinearities from the data allows us to study changes in sensitivity and temporal filtering independently for locations X and Y.

Local Contrast Induces Global Contrast Adaptation

We separately analyzed the spiking responses during episodes when locations X and Y were both stimulated with equal, low contrast (low/low condition), and when contrast at X was high, while contrast at Y remained the same as previously (high/low condition). Under the hypothesis that contrast adaptation occurs locally within the subfields, the filter and conditional nonlinearity at locations Y should stay the same when contrast switches only at locations X. For global contrast adaptation, on the other hand, the filter and conditional nonlinearity at locations Y are expected to display the same changes as for locations X.

Figure 2 shows the results for three representative ganglion cells. As expected, ganglion cells reacted to the contrast increases at locations X with a rapid increase in firing rate, followed by a slower decline over several seconds (Figure 2A). A comparison of the filters for X, obtained under high and low contrast at this location, revealed the typical effects of contrast adaptation (Baccus and Meister, 2002): the filters showed a shorter time-to-peak for higher contrast and often became more biphasic with a stronger secondary peak (Figure 2B). These changes in filter shape correspond to the accelerated response speed and reduced integration time of the neuron as well as to a relative increase in sensitivity to higher temporal frequencies.

For locations Y, contrast was the same during the two conditions, yet the filters displayed substantial changes (Figure 2C)

that were similar to those observed for locations X. During the high/low condition, the filters peaked earlier and were more biphasic as compared with the low/low condition, indicating that changes in temporal filtering occurred globally over the ganglion cells' receptive fields.

Changes in sensitivity were assessed by means of the conditional nonlinearities. For locations X, these nonlinearities showed the typical shift to the right for high contrast (Figure 2D), corresponding to reduced sensitivity. For locations Y, the conditional nonlinearities showed a similar shift (Figure 2E), indicating a corresponding decline in sensitivity when contrast was high at locations X. Together, these results indicate that contrast adaptation largely affected the cells' receptive fields in their entirety, rather than being confined to those regions in which contrast actually changed.

Closer inspection, however, revealed subtle differences between the contrast-induced changes of the filters at locations X and Y. First, the early part of the filters appeared to be regulated by local contrast. At locations Y, the filters for the two conditions remained nearly identical during the initial approach to the first filter peak, whereas at locations X, the two filters diverged much earlier. Second, the change in the biphasic shape of the filters was more pronounced at locations Y than at locations X, which was most apparent in the stronger increase of the secondary filter peak at locations Y. This finding appears quite counterintuitive: higher contrast led to more biphasic filters, but the amount of this change was stronger at locations where contrast in fact did not change. This gives the interaction between visual contrast and biphasic filter shape a flavor of "action at a distance"—an intriguing result to which we will return later.

These local adaptation effects did not depend on the specific assignment of locations X as those in which contrast changed. When we repeated the experiment with reversed roles of X and Y, so that contrast stayed constant at locations X and switched at locations Y, we found that the subtle local adaptation effects were also exchanged between X and Y. In particular, the stronger change in the biphasic shape was now observed for the filter at locations X rather than at locations Y (Figure S1A available online).

The sample cells shown in Figure 2 are all Off type, as the salamander retina is dominated by Off-type responses and contains only ~5%–10% On-type ganglion cells (Burkhardt et al., 1998; Segev et al., 2006). Previously, On cells in salamander retina were reported to have much weaker contrast adaptation effects than Off cells in terms of both sensitivity and temporal filtering (Kim and Rieke, 2001). The few On cells encountered in our recordings confirmed this observation. Yet, similar to the case with Off cells, the small observable adaptation effects in On cells were consistent with a global scope of contrast adaptation, as shown by two examples in Figure S1B. Because of the small number of recorded On cells and the weak contrast adaptation effects, all subsequent analyses in this work were restricted to Off-type ganglion cells.

Population analysis of all recorded Off-type ganglion cells corroborated the single-cell observations (Figure 3). As a general measure of changes in response speed, we assessed the time until the filter reached its minimal value and calculated the

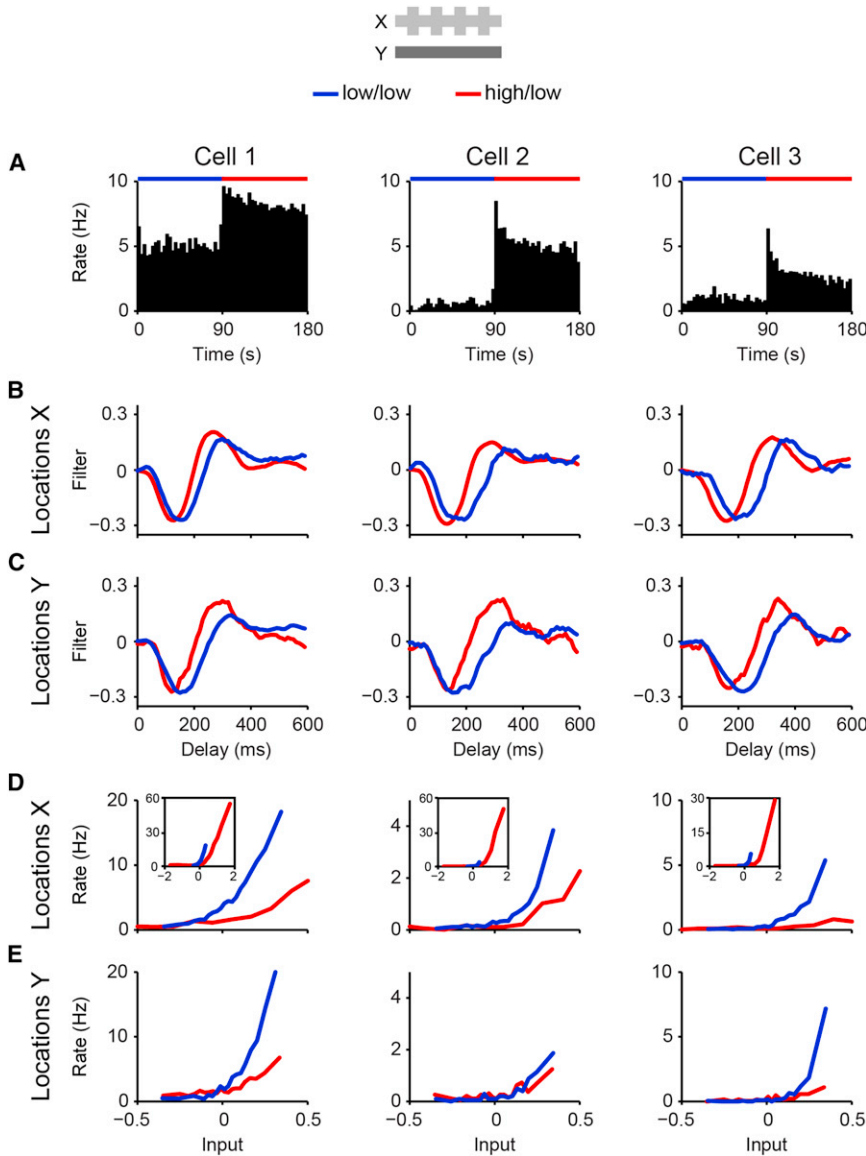


Figure 2. Filtering Characteristics and Nonlinearities of Ganglion Cells under Local Contrast Changes

Response characteristics from three sample ganglion cells are compared between the low/low contrast condition (blue lines) and the high/low contrast condition (red lines). The effects of reversing the roles of locations X and Y and data from two sample On cells are shown in Figure S1. (A) Firing-rate histograms averaged over all trials during the low/low condition (0–90 s) and during the high/low condition (90–180 s).

(B) Filters obtained for locations X.

(C) Filters obtained for locations Y. Note that filters from the high/low condition at Y are somewhat noisier than otherwise, reflecting the fact that spikes were primarily driven by the high-contrast stimulus component at locations X during this condition.

(D) Conditional nonlinearities obtained for locations X, shown over the input range spanned by the low-contrast stimulus. The insets show the nonlinearities over the range spanned by the high-contrast stimulus.

(E) Conditional nonlinearities obtained for locations Y.

In order to capture the very early part of the filter, we also computed the time until the filter reached a fixed threshold (chosen at -0.1 , close to half peak size for most filters) and called this the rise time of the filter (Figure 3B). For locations X, this rise time differed considerably by 27 ± 10 ms between the two contrast conditions ($p < 10^{-3}$), with statistically significant changes for 60 of the 68 cells. By contrast, although the rise time also changed for locations Y on the population level ($p < 10^{-3}$), this average change was only 4 ± 6 ms and thus was much smaller than for locations X ($p < 10^{-3}$), reaching significance for only four individual cells.

change in this time-to-peak for both locations X and Y. We found that most cells showed a comparable shift for both X and Y (X: 37 ± 13 ms; Y: 33 ± 14 ms; denoting mean \pm SD, as in all subsequent quantifications of population data; Figure 3A), supporting a global change in response speed. In fact, while the time-to-peak experienced significant changes on the population level for both locations X and Y ($p < 10^{-3}$ in both cases, assessed here and in subsequent population analyses by a Wilcoxon signed-rank test), the shift values did not differ significantly between X and Y ($p = 0.31$). We further assessed the statistical significance of the observed changes for each cell individually by partitioning the data, repeating the analysis for each data fraction, and performing a Wilcoxon rank-sum test on the obtained sets of values. For locations X, the shift in time-to-peak was significant for 63 of the 68 analyzed cells, and for locations Y, it was significant for 51 cells.

This confirmed that the kinetics of the early filter part depended mostly on local contrast.

To assess changes in sensitivity at locations X and Y, we computed the sensitivity during the low/low condition (S_1) and the high/low condition (S_2) as the maximal values of the conditional nonlinearities (Figures 2D and 2E) over the input range that was spanned by the low-contrast stimuli. The change in sensitivity was then measured as the ratio of S_1 and S_2 (Figure 3C). Values close to unity of this ratio indicate no or little change in sensitivity, and values above unity stand for increased sensitivity during the low/low condition as compared with the high/low condition. For both X and Y, sensitivity was strongly increased during the low/low condition ($S_1/S_2 = 2.9 \pm 1.2$ and 2.8 ± 1.5 for X and Y, respectively; $p < 10^{-3}$ in both cases), yet there was no significant difference between the two stimulus components ($p = 0.39$), indicating a mostly global scope of sensitivity changes.

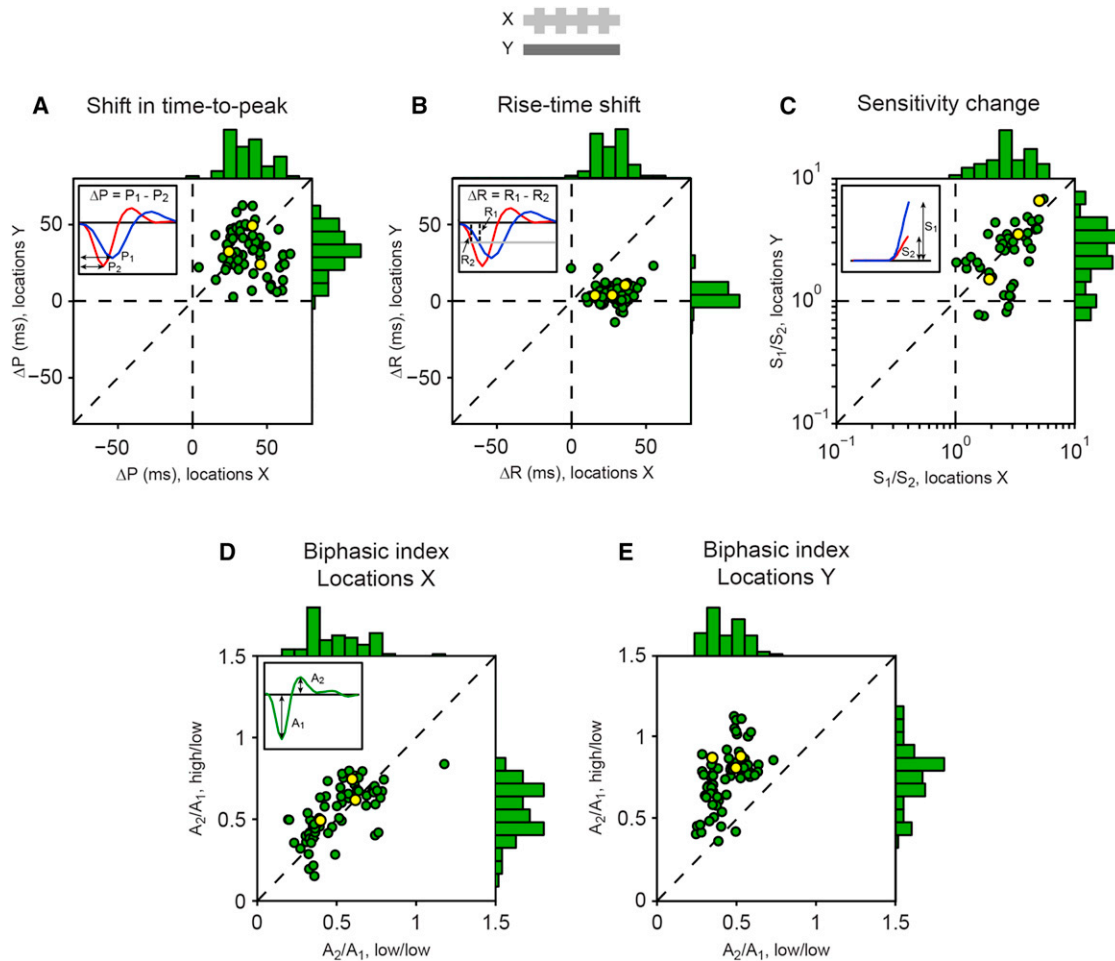


Figure 3. Population Analysis of Changes in the Filters and Sensitivity in Response to Local Contrast Changes

(A) Shift in time-to-peak of the filters between the low/low and high/low conditions, calculated as depicted in the inset, compared for locations X and locations Y for all recorded ganglion cells. The dashed diagonal line indicates identical magnitudes of the shift. Here and in subsequent panels, the yellow data points show the data from the three sample cells of Figure 2. The characteristics of a subset of cells showing significantly stronger time-to-peak shifts for locations X are further analyzed in Figure S2.

(B) Comparison of rise-time shifts. Rise time was calculated as the time until the filter crossed a threshold of -0.1 from above, as depicted in the inset.

(C) Comparison of sensitivity change, calculated (as depicted in the inset) as the ratio of the maximal values in the conditional nonlinearities over the range spanned by the low-contrast stimulus. To reduce the effect of noise, only data points for which these sensitivity measures reached at least 0.5 Hz were included in the plot.

(D) Biphasic indices for locations X, compared for the low/low and the high/low conditions. The indices were calculated as the ratio of filter peaks as depicted in the inset.

(E) Same as (D), but for locations Y.

Finally, we assessed changes in filter shape by calculating a biphasic index (Zaghloul et al., 2007) as the amplitude ratio of the second versus the first peak of the filter. This index yields values around zero for a mostly monophasic filter with a negligible secondary peak, and values around unity for strongly biphasic filter shapes with first and second peaks of comparable magnitude. For locations X (Figure 3D), we found that the biphasic index was on average slightly larger during the high/low condition (high/low: 0.54 ± 0.16 ; low/low: 0.50 ± 0.18 ; $p < 10^{-3}$). For locations Y (Figure 3E), the biphasic index was also larger during the high/low condition (high/low: 0.76 ± 0.18 ; low/low: 0.44 ± 0.11 ; $p < 10^{-3}$), and this effect was much more pronounced than for locations X ($p < 10^{-3}$). This confirmed the

counterintuitive observation that these changes in filter characteristics were stronger for locations in the receptive field where contrast did not change.

Note that besides the dominant global contrast adaptation effects, analysis of both the change in time-to-peak (Figure 3A) and the change in sensitivity (Figure 3C) revealed distinct subgroups of cells with local changes that were stronger at locations X than at locations Y. In fact, 16 of the 68 cells showed a significantly larger shift in time-to-peak for X, indicative of local adaptation. Yet, this subset of cells still also showed some level of global adaptation, as the time-to-peak at Y also changed significantly for this subset on the population level ($p < 10^{-3}$) as well as for five of the 16 cells on the single-cell level.

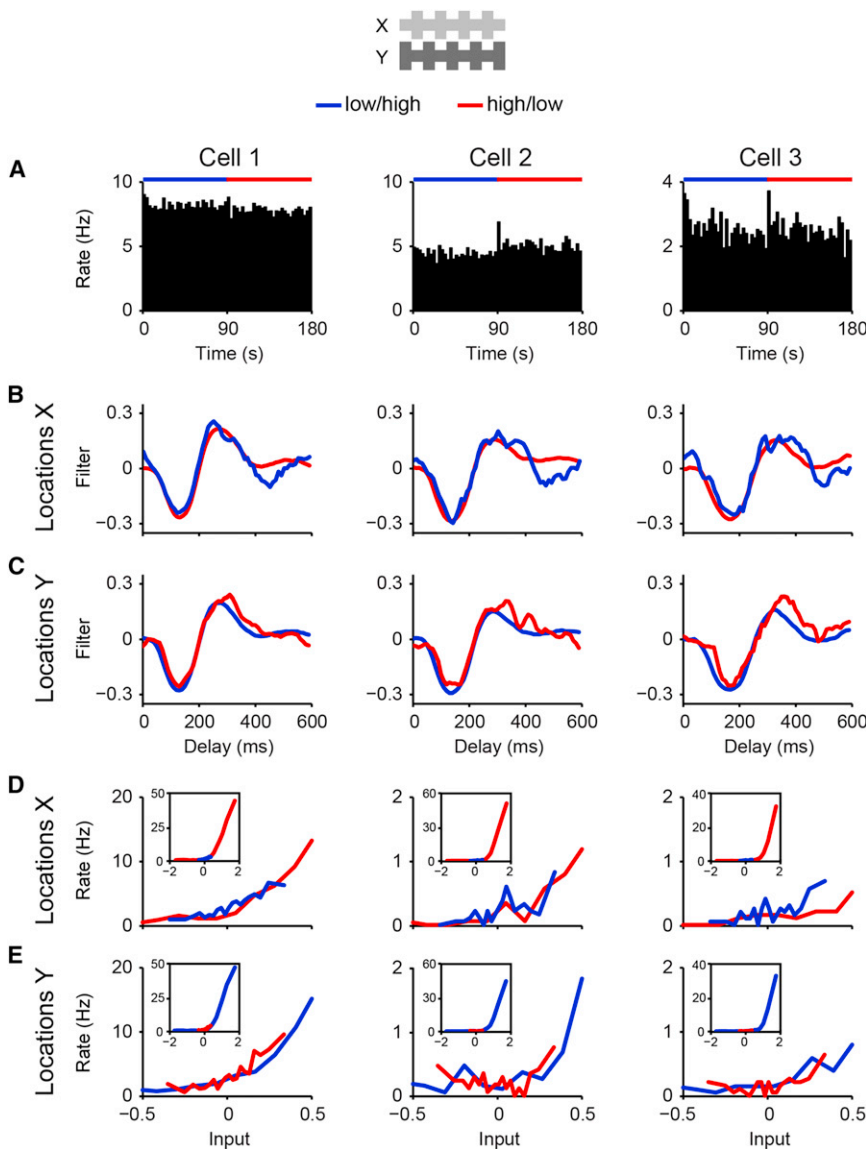


Figure 4. Filtering Characteristics and Nonlinearities of Ganglion Cells under Local Contrast Changes with Constant Global Contrast

Data are shown for the same three sample ganglion cells presented in Figure 2. In all plots, data from the low/high contrast (high contrast at Y; blue lines) and high/low contrast (high contrast at X; red lines) conditions are compared.

(A) Firing-rate histograms averaged over all trials during the low/high condition (0–90 s) and high/low condition (90–180 s).

(B) Filters obtained for locations X.

(C) Filters obtained for locations Y.

(D) Conditional nonlinearities obtained for locations X, shown over the input range spanned by the low-contrast stimulus. The insets show the nonlinearities over the range spanned by the high-contrast stimulus.

(E) Same as (D), but for locations Y.

by opposing contrast changes at locations Y. We therefore also tested a modified stimulus and performed experiments in which high and low contrast alternated at locations X and Y in antiphase, with the aim of keeping global contrast constant over each ganglion cell's receptive field.

Figure 4 displays the results from this experiment for the same three cells shown in Figure 2. Average firing rates during the low/high condition with low contrast at X and high contrast at Y were approximately the same as those during the high/low condition with reversed contrast assignment (Figure 4A). This confirmed that the two conditions provided about the same total contrast for each of these cells. Note, though, that brief increases in firing rate could be observed for some cells just after

Furthermore, this subset of cells had substantially weaker sensitivity changes at Y as compared with the remaining cells ($p < 10^{-3}$), and, as shown in Figure S2, encompassed those cells that showed particular local changes in sensitivity. Moreover, this group of cells had comparatively large receptive fields (average diameter $441 \pm 86 \mu\text{m}$ within this subset versus $316 \pm 115 \mu\text{m}$ for the remaining cells; $p < 10^{-3}$; Figure S2F) and relatively small biphasic indices (0.35 ± 0.09 averaged over X and Y for the low/low condition versus 0.51 ± 0.15 for the remaining cells; $p < 10^{-3}$). Together, these findings suggest that specific subclasses of ganglion cells exist, which have substantial local effects of contrast adaptation.

Keeping Global Contrast Constant Strongly Reduces Adaptation Effects

The largely global scope of contrast adaptation led us to hypothesize that contrast changes at locations X could be counteracted

a transition between the two conditions, here apparent for cell 2 and cell 3. Such a transient increase in firing rate was previously interpreted as a sign of local adaptation (Brown and Masland, 2001); however, as we will discuss in more detail below, an alternative explanation is provided by spatial nonlinearities within the receptive field.

Most importantly, both the filters (Figures 4B and 4C) and the nonlinearities (Figures 4D and 4E) were now much more similar for the two conditions, confirming that filtering characteristics and sensitivity are mostly regulated by global contrast, not by local contrast. Yet, subtle effects of local contrast persisted, as is evident in some of the examples. The early filter part tended to be slightly faster when local contrast was high at the respective location, and the filters were slightly more biphasic when local contrast was low.

These findings were again confirmed by population analysis (Figure 5). In contrast to the previous experiment, the shifts in

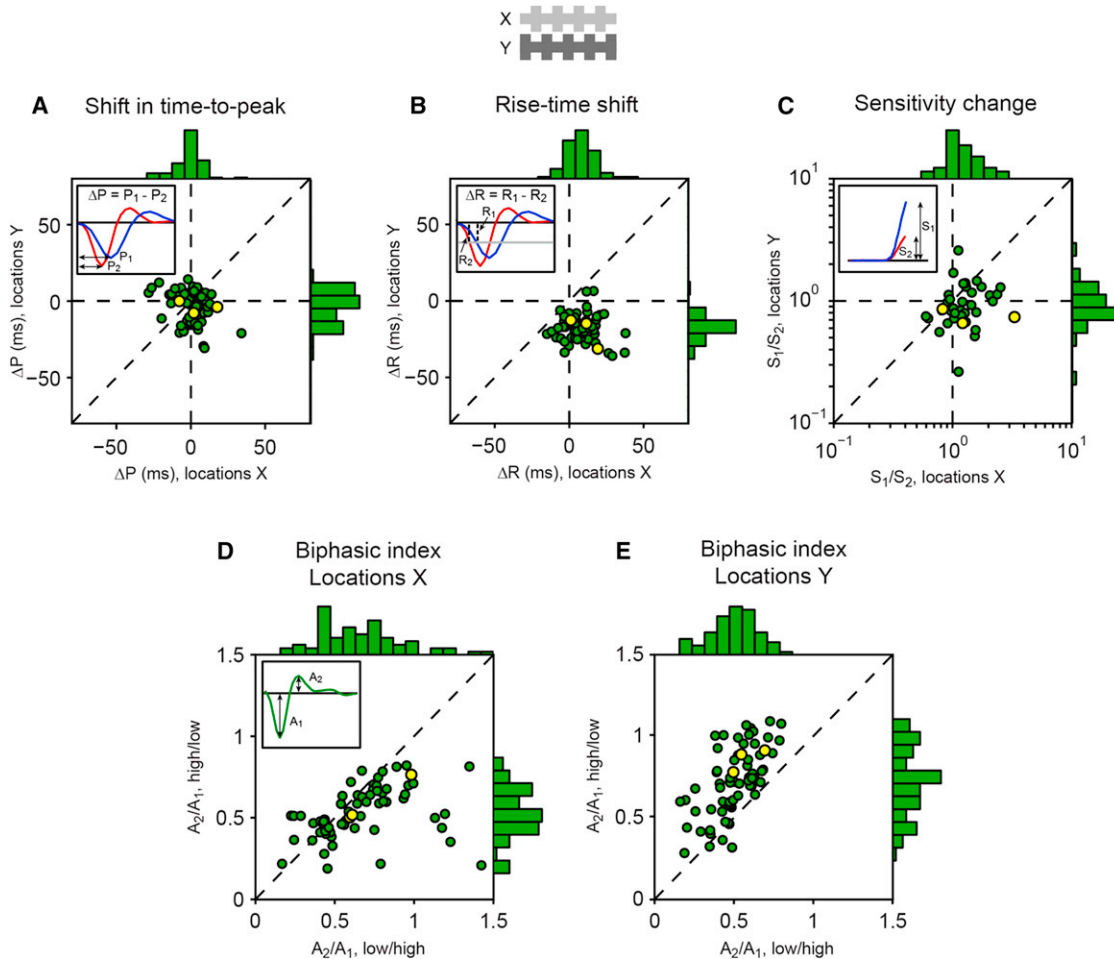


Figure 5. Population Analysis of Changes in the Filters and Sensitivity in Response to Local Contrast Changes with Constant Global Contrast As depicted in the insets, changes in filters and sensitivity were calculated in the same way as for Figure 3. Yellow data points show data for the examples in Figure 4.

(A) Shift in time-to-peak of the filters compared for locations X and Y for all recorded ganglion cells. The shift in time-to-peak was calculated as $\Delta P = P_1 - P_2$, with P_1 and P_2 denoting the time-to-peak for the low/high and high/low conditions, respectively.

(B) Comparison of rise-time shifts, calculated as $\Delta R = R_1 - R_2$, with R_1 and R_2 denoting the rise time for the low/high and high/low conditions, respectively. The data show that the rise time for X was typically shorter when contrast was high at X ($\Delta R > 0$, i.e., $R_2 < R_1$), whereas the rise time for Y was shorter when contrast was high at Y ($\Delta R < 0$, i.e., $R_1 < R_2$).

(C) Comparison of sensitivity changes, calculated as S_1/S_2 . As in Figure 3C, only cells for which the sensitivity measures reached at least 0.5 Hz were included in the plot.

(D) Biphasic indices for locations X compared for low/high and high/low conditions.

(E) Same as (D), but for locations Y.

time-to-peak (Figure 5A) were now much smaller and did not deviate significantly from zero for either locations X ($p = 0.82$) or locations Y ($p = 0.06$). The shift in rise time, on the other hand, still showed a small yet systematic effect for both X and Y (Figure 5B): during the low/high condition, rise times were longer for locations X as compared with the high/low condition (average shift 8 ± 10 ms; $p < 10^{-3}$) and shorter for locations Y (average shift -17 ± 8 ms; $p < 10^{-3}$), confirming that larger local contrast led to shorter rise times.

Changes in sensitivity were much smaller than observed in the previous experiment ($p < 10^{-3}$ for both X and Y), confirming the primary dependence of sensitivity on global contrast (Figure 5C).

Yet, an additional, small local component now became apparent in the population data, as can be seen in the following ways: First, the changes in sensitivity between the low/high and high/low condition were significant for locations X ($p < 0.01$) but not for locations Y ($p = 0.09$), the latter potentially because of fluctuations in overall sensitivity caused by residual differences in global contrast. Second, the fact that the data points in Figure 5C lie preferentially below the identity line means that S_1/S_2 was systematically larger at X than at Y ($p < 10^{-3}$), which demonstrates that sensitivity at X increased systematically as compared with sensitivity at Y when switching from the high/low to the low/high condition and vice versa. This shows that

sensitivity increased slightly but systematically with decreasing local contrast.

Finally, the measured biphasic indices confirmed the observation of an action at a distance by local contrast: filters were more biphasic when local contrast was low at the corresponding location and high at other locations. Concretely, for locations X (Figure 5D), biphasic indices were larger during the low/high condition (low/high: 0.66 ± 0.27 ; high/low: 0.53 ± 0.16 ; $p < 10^{-3}$) and for locations Y (Figure 5E) during the high/low condition (high/low: 0.72 ± 0.21 ; low/high: 0.50 ± 0.15 ; $p < 10^{-3}$). In the following section, we will therefore investigate this intriguing aspect in more detail.

Adaptation Effects Persist under Inhibition Block

One potential explanation for the action at a distance is that filter changes are mediated by lateral inhibitory interactions. We therefore tested whether blocking inhibition in the retinal circuit influenced the observed changes in filter shape. As an example, Figures 6A and 6B show the measured filters for cell 1 of Figures 2 and 4 after applying a cocktail of strychnine (5 μ M), picrotoxin (150 μ M), and bicuculline (20 μ M) to the retina to block inhibitory neurotransmission. Yet, the changes in filter shape between the different contrast conditions remained qualitatively the same as in the control conditions for this cell.

Population analysis confirmed this finding. Filters under inhibition block still had shorter time-to-peak during the high/low condition as compared with the low/low condition (time-to-peak shift 21 ± 12 ms for X and 20 ± 11 ms for Y; $p < 10^{-3}$ in both cases; data not shown), but time-to-peak values did not change when global contrast stayed constant ($p = 0.08$ for X; $p = 0.59$ for Y; data not shown). More importantly, the filters were still more biphasic when contrast was high at the other locations. When contrast increased only at X (Figure 6C), biphasic indices did not change significantly for locations X (high/low: 0.82 ± 0.16 ; low/low: 0.81 ± 0.20 ; $p = 0.49$), but increased substantially for locations Y (high/low: 0.94 ± 0.19 ; low/low: 0.82 ± 0.18 ; $p < 10^{-3}$). When contrast changed at both X and Y in antiphase (Figure 6D), biphasic indices were larger whenever the corresponding local contrast was low (for X: low/high: 0.94 ± 0.32 ; high/low: 0.74 ± 0.19 ; $p < 10^{-3}$; for Y: high/low: 1.04 ± 0.35 ; low/high: 0.73 ± 0.17 ; $p < 10^{-3}$).

Thus, blocking inhibition did not qualitatively alter the contrast-dependent changes in filter shape. However, it did have a profound general effect on filter shapes. Compared with control conditions (Figures 3D and 3E and Figures 5D and 5E, respectively), the biphasic indices were systematically larger under the inhibition block ($p < 10^{-3}$ for both X and Y in both experiments and all contrast conditions; Figures 6C and 6D). This indicated that the biphasic shape is connected to the overall strength of the excitatory activation, which increases when inhibition is blocked. Thus, a plausible mechanism is that the secondary peak in the filter results from a (noninhibitory) negative feedback mechanism, triggered by sufficiently strong activation. There are several candidates for such negative feedback, including synaptic depression and activity-dependent ionic conductances in the ganglion cells. We therefore explored the consequences of such feedback mechanisms on contrast adaptation.

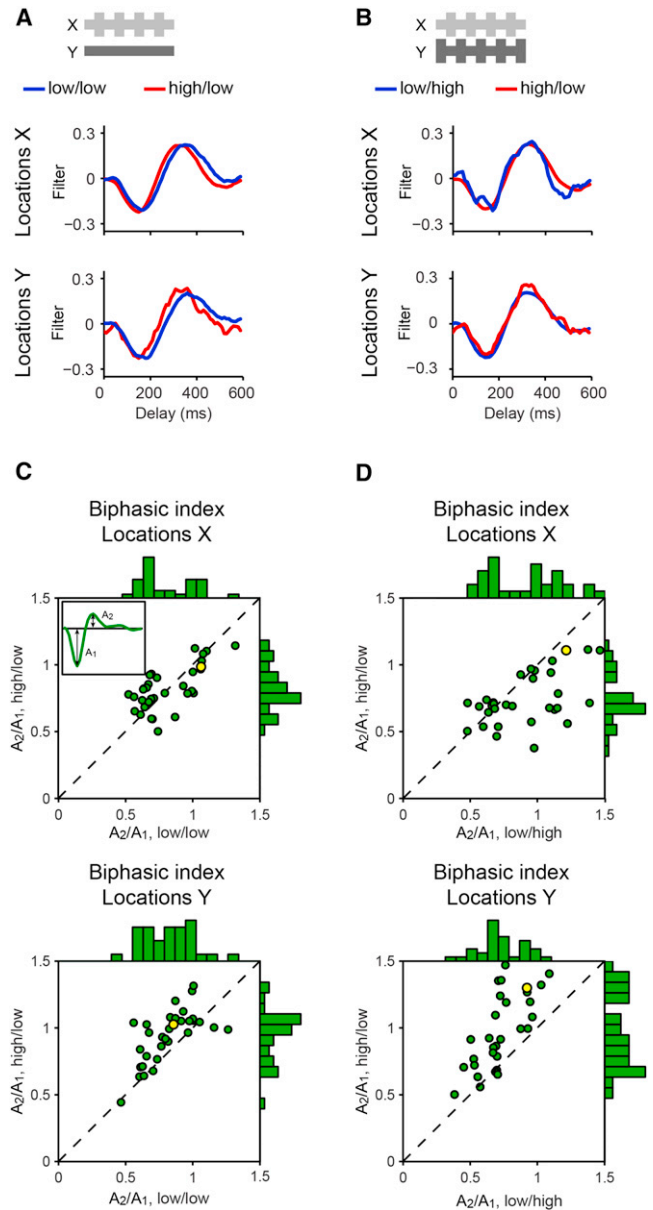


Figure 6. Effect of Inhibition Block on Contrast-Induced Changes in Filter Shape

(A) Filters obtained under inhibition block for the ganglion cell shown as cell 1 in Figures 2 and 4 in response to the stimulus with contrast changes only at X (cf. Figures 2B and 2C).

(B) Filters obtained under inhibition block for the same cell for the stimulus with contrast changes at X and Y in antiphase (cf. Figures 4B and 4C).

(C) Biphasic indices at locations X (top) and locations Y (bottom) under inhibition block for the stimulus with contrast changes only at X (cf. Figures 3D and 3E).

(D) Biphasic indices at locations X (top) and locations Y (bottom) under inhibition block for the stimulus with contrast changes at X and Y in antiphase (cf. Figures 5D and 5E). The yellow data points in (C) and (D) show data from the sample cell of (A) and (B).

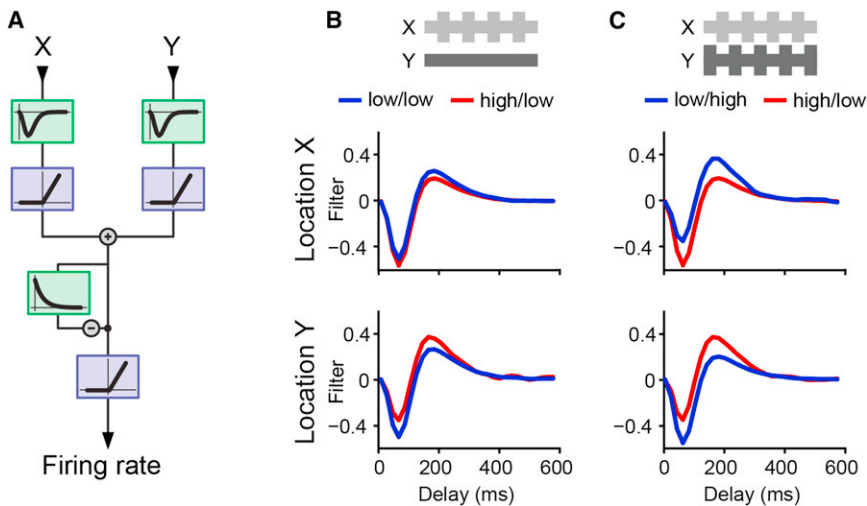


Figure 7. Nonadapting Model that Explains the Effects of Other Locations on Filter Shape

(A) Layout of the model, as explained in the text. (B) Filters obtained from model simulations for locations X and Y for the stimulus with contrast changes only at X.

(C) Filters obtained from model simulations for locations X and Y for the stimulus with contrast changes at X and Y in antiphase.

The above mechanism relies on the fact that the feedback is sandwiched between the two nonlinearities. It is not essential, however, that the feedback acts after summation. In fact, because of the linearity of the feedback filter, a model with two local feedback stages

A Nonadapting Model for Contrast-Induced Changes in Filter Shapes

To investigate how contrast may affect the filter shapes in the presence of activity-dependent feedback, we set up a simple computational model of a retinal ganglion cell that pools inputs from two locations X and Y (Figure 7A). In the model, the ganglion cell receives these inputs via two bipolar cells, modeled as monophasic Off-type temporal filters for simplicity. Subsequent synaptic transmission imposes a threshold-linear transformation on the two filtered signals before they are summed by the ganglion cell. A low-pass-filtered version of the summed signal is then subtracted, implementing a negative feedback. Finally, another threshold-linear transformation represents the spiking threshold of the ganglion cell and yields the cell's firing rate.

As with the experimental data, we used spike-triggered-average analysis to obtain filter shapes for this model. Despite the simplicity of the model and the lack of any explicit adaptation dynamics, it produced intriguing local changes in the biphasic shape of the filters that were qualitatively similar to those observed in the experiments. The change in biphasic shape was particularly strong at location Y when contrast only changed at X (Figure 7B). Furthermore, for contrast changes in antiphase, filters were more biphasic when local contrast was high at the other location (Figure 7C). This shows that the combined effect of negative feedback and local nonlinearities in the ganglion cell receptive field can explain the local changes in the biphasic filter shape.

How does the model lead to these changes in filter shape? As it is the feedback that causes the secondary peak in the filter for this model, the size of this peak is determined by how effective this feedback component is. Because of the local nonlinearity before the feedback, the feedback acts only to suppress activity, never to enhance it. This suppression is most effective when it coincides with strong positive activation; otherwise the feedback effect is limited because activity cannot be suppressed below zero, as enforced by the global nonlinearity. Thus, the feedback is more effective when more activity is supplied via parallel channels, that is, when contrast is high at other locations.

just before summation of the local signals is mathematically equivalent to the model of Figure 7A, as long the feedback acts after the local nonlinearities. This allows us to interpret the feedback mechanistically not only as an intrinsic process in the ganglion cell but also as a process that occurs during synaptic transmission. For example, the local nonlinearity could result from a nonlinear dependence of transmitter release on the pre-synaptic potential (Baccus et al., 2008; Werblin, 2010). Subsequent negative feedback might then result from synaptic depression (Burrone and Lagnado, 2000; Singer and Diamond, 2006; Li et al., 2007; Jarsky et al., 2011), triggered by transmitter release and thus occurring after the local nonlinearity.

Comparison with Previous Reports of Local Contrast Adaptation

In contrast to our finding of largely global contrast adaptation effects on ganglion cell sensitivity, ganglion cells in rabbit retina were previously reported to display local adaptive sensitivity changes under local stimulation within the receptive field (Brown and Masland, 2001). These findings were based on cross-adaptation experiments in which stimulation was suddenly switched from one part of the receptive field to another. Following the switch, ganglion cells showed a brief, transient increase in firing rate, as also observed in some examples in Figure 4. For linear spatial receptive fields, the simplest interpretation is that the newly stimulated location was not yet adapted and thus had higher sensitivity for a brief period. However, given the importance of local nonlinearities within the receptive field for signal processing under changing contrast (Figure 7), as well as the ubiquity of such nonlinearities in the salamander retina (Bölinger and Gollisch, 2012), one is led to ask whether local nonlinear processing affects cross-adaptation experiments as well.

We thus explored a simple nonlinear ganglion cell model without any adaptation mechanism (Figure 8A), and found that it could produce response transients after a switch in stimulus location similar to those reported experimentally. The model has two parallel input signals, here corresponding to two locations within the cell's receptive field. Each input signal is temporally filtered and then nonlinearly transformed by a

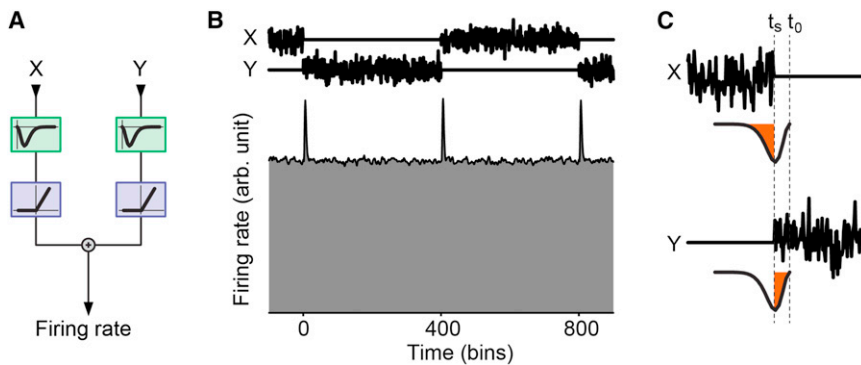


Figure 8. Nonadapting Model that Explains Firing-Rate Transients after Switches in Stimulus Location

(A) Layout of the model, as explained in the text. (B) Firing-rate histogram in response to switching the input location of a white-noise stimulus between X and Y. Examples of the stimulus sequence are shown at the top. (C) Schematic explanation of the firing-rate transients. At a time t_0 shortly after the switch in stimulus location at time t_s , the response is affected by signals from both input channels because of the extended integration time given by the temporal filter. Each channel contributes according to the overlap of the filter with the stimulus sequence, as indicated by the shaded regions within the filters shown below the stimulus sequences.

threshold-linear function. To mimic the cross-adaptation experiment, the model was stimulated by a white-noise sequence that switched between the two input channels. Despite the apparent absence of local adaptation dynamics, the firing rate of the model displayed a brief, transient increase in response to a switch (Figure 8B).

The response transients after the switch were brief, corresponding approximately to the model's integration time (as defined by the extent of the temporal filter). In fact, this corresponds to the previous experimental study (Brown and Masland, 2001) in which, after a switch in stimulus location, the increases in firing rate were notably brief, lasting for only some hundreds of milliseconds, which is a typical timescale for ganglion cell temporal filters. In experiments where global contrast was switched, on the other hand, the same cells had displayed much longer response transients.

How the model produces the response transients can be understood as follows: Since each input channel integrates the stimulus over some temporal window, there is a brief period just after a switch when both input channels contribute signals to the output (Figure 8C). Since the signals are nonlinearly transformed before summation, their combined effect need not sum to the same baseline activation, as when only one input channel contributes, but can be higher or lower depending on the shape of the local nonlinearity. For the chosen threshold-linear transformation, the combined signal of both input channels turns out to be larger than baseline, as derived in the Supplemental Text.

This model analysis shows that brief response transients in the considered cross-adaptation experiments can be expected independently of local contrast adaptation effects and do not necessarily provide evidence for local adaptation, unless the considered cell is known to have linear stimulus integration or the response transients exceed the integration time of the cell. Thus, when stimulus integration may be nonlinear, an important ingredient for identifying local adaptation through a cross-adaptation experiment is a comparison of time scales between the response transients and the cell's integration time.

DISCUSSION

When visual contrast changes, retinal ganglion cells adjust their sensitivity and temporal filtering characteristics. In this work, we

investigated whether these different adaptive modifications occur locally within the receptive field of a ganglion cell or whether they are properties of the receptive field in its entirety. To do so, we used a stimulus layout that contained contrast changes in local subfields (Figure 1). We found that ganglion cells showed strong adaptation effects also for subfields where contrast did not change (Figures 2 and 3), and that adaptation effects were comparatively weak when local contrast changed in a way that kept global contrast constant (Figures 4 and 5). This indicated that contrast adaptation acts primarily in a global manner over the entire receptive field. A small subset of ganglion cells, however, also showed considerable local adaptation effects, suggesting that the relative importance of local and global adaptation may vary with ganglion cell subtype. Furthermore, we also found subtle yet intriguing local adaptation components. First, small local sensitivity changes were uncovered when global contrast stayed constant (Figure 5C). Second, the early part of the stimulus filter depended primarily on local contrast (Figures 2 and 3B). Third, the changes in biphasic filter shape displayed a surprising local component that depended on contrast at other locations in the receptive field (Figures 2, 3D, 3E, 5D, and 5E). This effect did not qualitatively depend on inhibitory signaling in the retinal circuitry (Figure 6). Instead, a simple computational model, based on negative feedback sandwiched between a local and a global nonlinear processing stage, could explain this seemingly paradoxical action at a distance (Figure 7). Finally, we showed that local nonlinearities, as an alternative to local contrast adaptation as was previously assumed, may provide an explanation for the response transients in cross-adaptation experiments (Figure 8).

Our analysis focused on the steady-state response after a switch in visual contrast, and thus did not probe the temporal dynamics of adaptation. Previous studies with spatially uniform stimuli showed that temporal filters adjust nearly instantaneously, whereas sensitivity shows instantaneous changes as well as further adjustments over the course of several seconds (Baccus and Meister, 2002). The instantaneous components are also referred to as contrast gain control to distinguish them from slower adaptation components. By analogy, it seems likely that the local and global changes in the filters observed here also occur immediately after the contrast switch, whereas the measured changes in sensitivity result from a combined effect

of the fast and slow contrast adaptation processes. In addition, after a switch to low visual contrast, sensitivity may transiently increase for some cells (Kastner and Baccus, 2011), but this sensitization does not affect the steady-state response analyzed here.

The immediate effect on the temporal filters is consistent with the type of model presented in Figure 7, where the contrast dependence of the filter shapes did not correspond to slow parameter changes within an LN model, but rather resulted from mapping a nonadapting model with several linear and nonlinear stages onto the standard two-stage LN model, which provides readily interpretable measures of temporal filtering and sensitivity and serves to connect the results to previous studies (Baccus and Meister, 2002; Wark et al., 2007). Similarly, rapid-adaptation phenomena have previously been accounted for by extended nonlinear models without the need to invoke contrast-dependent parameter changes (Borst et al., 2005; Gauthier and Reinagel, 2007). As computational tools progress, it may ultimately be possible to directly interpret experimental data through such nonlinear models that directly incorporate the relevant operations for contrast adaptation (Baccus and Meister, 2002).

Importance of Local Nonlinear Processing

The models that we considered for explaining the local changes of filter shapes (Figure 7) and the response transients in cross-adaptation experiments (Figure 8) depend critically on local nonlinearities within the receptive field of ganglion cells. This highlights the importance of understanding receptive field nonlinearities (Schwartz and Rieke, 2011), which have also been connected to several computational tasks performed by the retina (Gollisch and Meister, 2010). It has long been known that the retina contains ganglion cells with linear and nonlinear receptive fields (Enroth-Cugell and Robson, 1966). In the salamander retina, nonlinear receptive fields seem to be the rule (Bölinger and Gollisch, 2012).

Recordings and modeling of the synaptic connection between rod bipolar cells and amacrine cells have recently shown that contrast adaptation at this synapse is shaped by the tight connection of nonlinear signal transfer and synaptic depression (Jarsky et al., 2011). Similarly, a biophysical model of synaptic depression at the bipolar cell terminal can provide an accurate description of contrast adaptation dynamics in retinal ganglion cells (Ozuyal and Baccus, 2012). These models rely on a nonlinear transformation of bipolar cell signals, which converts information about the signal variance into a change in the signal mean, and a subsequent adaptation mechanism. It thus seems feasible that these biophysical mechanisms underlie the local nonlinearity and the subsequent phenomenological feedback operation of Figure 7A.

Mechanisms

Our results provide constraints on the cellular and synaptic mechanisms underlying contrast adaptation in the retina. The observed global sensitivity changes of ganglion cells could result from mechanisms intrinsic to the cells, for example inactivation of sodium channels (Kim and Rieke, 2003) or recruitment of potassium currents (Weick and Demb, 2011). Indeed, it was

previously reported that sensitivity changes are more pronounced in the spiking responses of ganglion cells than in their synaptic inputs (Kim and Rieke, 2001; Zghloul et al., 2005). On the other hand, some bipolar cells in the salamander retina show contrast adaptation themselves (Rieke, 2001; Baccus and Meister, 2002), which might contribute to the local adaptation effects observed in a subset of ganglion cells. Furthermore, synaptic depression at the bipolar cell terminals is likely to contribute to local contrast adaptation effects.

Yet, perhaps counterintuitively, synaptic depression can also mediate global adaptation. If, for example, the basal rate of neurotransmitter release is sufficiently high, depletion of the vesicle pool can lower the basal transmitter release rate (Manookin and Demb, 2006; Beaudoin et al., 2008) and thereby lead to a lower baseline of the postsynaptic membrane potential in the adapted state. Indeed, following a switch to high contrast, a slow hyperpolarization of the membrane potential has been observed, accounting for sensitivity changes that occur on the scale of a few seconds (Baccus and Meister, 2002; Manookin and Demb, 2006). As this reduction in the baseline potential also makes it harder for other inputs to trigger a spike, input channels without a change in contrast also experience a reduction in sensitivity, accounting for the global scope of sensitivity changes.

In contrast to such a baseline shift, a reduction in the gain of transmitter release following synaptic depression would have a multiplicative effect on the postsynaptic potential and thus result in local sensitivity changes, as the reduced gain of one input component does not reduce the effectiveness of other input components. It seems likely that such gain changes and baseline shifts go hand in hand, and it remains to be investigated how strong the relative contributions of the resulting local and global adaptation effects in detailed synaptic depression models would be. Note that small local sensitivity changes (cf. Figure 5C) may become more relevant for other adaptation phenomena. In particular, the more subtle pattern adaptation under variations in spatiotemporal stimulus statistics (Hosoya et al., 2005; Ölveczky et al., 2007) suggests local changes in sensitivity, which may result from synaptic depression (Gollisch and Meister, 2010). Further note that the relative contributions of these different mechanisms may differ between the salamander retina (as used in the present study as well as in several previous investigations of contrast adaptation [Smirnakis et al., 1997; Rieke, 2001; Baccus and Meister, 2002]) and mammalian retinas (such as in the guinea pig [Zghloul et al., 2005; Manookin and Demb, 2006; Beaudoin et al., 2007; Weick and Demb, 2011] and rabbit [Brown and Masland, 2001]).

Regarding changes in filter shape, the local effect on the early rise time of the filter suggests that stronger local stimulation leads to accelerated local signaling from bipolar cells. This local component might then later be masked by other, primarily global changes in filter shape. For these later changes, models that combine local nonlinearities and feedback filters provide good candidates; they can explain why certain filter changes are stronger at locations where contrast does not change (Figure 7), and they leave the early filter part unaffected because the feedback is expected to act with some temporal delay.

Functional Relevance

Whether contrast adaptation occurs locally within or globally over a ganglion cell's receptive field has important functional consequences. Adaptation after spatial pooling has the advantage that a more reliable estimate can be obtained about the prevailing stimulus context, and local fluctuations of stimulus statistics have less impact. In this respect, future studies might investigate whether the spatial scale of adaptation depends on the light level or on the spatial statistics of visual stimuli, analogous to the observation that the temporal scale of contrast adaptation is dynamically adjusted according to the temporal structure of contrast changes (Wark et al., 2009). It has already been shown, for example, that the characteristics and mechanisms of contrast adaptation differ under scotopic and photopic conditions (Beaudoin et al., 2008), though contrast-induced changes in temporal filtering are independent of mean luminance over some range (Mante et al., 2005).

Distinguishing between local and global adaptation is also important for understanding how a ganglion cell responds to complex visual stimuli that may contain several objects within a receptive field. With global sensitivity changes, the presence of one object strongly affects the sensitivity to another object at a different location in the receptive field. This means that the ganglion cell becomes particularly selective to the object of highest contrast in a winner-take-all fashion, at the expense of detectability of weaker objects, which might allow downstream processing to focus on the most salient visual features (Itti and Koch, 2001). Locally adapting cells, on the other hand, allow each object to be processed according to the object's own level of contrast, thus preserving sensitivity to weak stimuli even in the presence of other, high-contrast objects.

Global changes in sensitivity are furthermore connected to the encoding of small moving objects that travel through the receptive field. It has been shown that the retinal activity elicited by a moving object marks the leading edge of the object rather than the trailing edge, thus anticipating the object's motion trajectory and counteracting temporal delays that occur from the phototransduction process (Berry et al., 1999). Mechanistically, this motion anticipation has been suggested to rely on contrast-dependent sensitivity changes: the strongest response is elicited when the object first enters the receptive field and sensitivity is still high, whereas the subsequent reduction in sensitivity partly suppresses the response as the object proceeds through the receptive field. This suppression only works if activation of some part of the receptive field also changes sensitivity in other parts, that is, if contrast adaptation acts on the entire receptive field.

Application to Other Systems

Adaptation to stimulus variance is a common feature of sensory systems and has also been investigated in different parts of the auditory system (Kvale and Schreiner, 2004; Dean et al., 2005; Nagel and Doupe, 2006; Rabinowitz et al., 2011) and in the somatosensory system (Garcia-Lazaro et al., 2007; Maravall et al., 2007). Because most sensory systems also display substantial convergence of parallel signaling pathways, the question arises as to whether at a given stage of sensory processing, adaptation occurs locally over individual input pathways or

globally as a feature of the neuron under investigation. The approach used in this work, based on continuous, independent activation of different pathways and local changes of their individual input statistics, is not specific to visual processing and thus may help elucidate the characteristics of adaptation in other systems. The most direct application of this approach may be possible in the auditory system, where neurons have been shown to display adaptive changes in sensitivity and temporal filtering quite similar to the contrast adaptation effects of the retina (Nagel and Doupe, 2006; Dahmen et al., 2010). These auditory neurons are typically described by their spectro-temporal receptive fields. Investigating whether the different effects of variance adaptation act locally or globally in frequency space (Gollisch and Herz, 2004) is thus directly analogous to the present study of the spatial scope of contrast adaptation in the retina.

EXPERIMENTAL PROCEDURES

Electrophysiology and Visual Stimulation

Spike trains of retinal ganglion cells were recorded from isolated retinas of axolotl salamanders (*Ambystoma mexicanum*; pigmented wild-type) with 60-channel multielectrode arrays as described previously (Bölinger and Gollisch, 2012). Retinas were prepared under infrared illumination using a stereomicroscope equipped with night-vision goggles. During the recordings, retinas were superfused with oxygenated Ringer's solution at room temperature (20°C–22°C). All experimental procedures were performed in accordance with institutional guidelines of the Max Planck Society and the University Medical Center Göttingen.

Visual stimuli were projected onto the retina with a gamma-corrected CRT monitor at a refresh rate of 100 Hz and standard optics. The low- and high-contrast conditions used in the experiments had the same mean light intensity in the photopic range and contrast levels of 20% and 97%, respectively. Spatial receptive fields were obtained from the spike-triggered average under stimulation with spatiotemporal white noise. Details of the experimental methods can be found in [Supplemental Experimental Procedures](#).

Analysis

The filters and nonlinearities for the different contrast conditions were obtained by a spike-triggered-average analysis as described previously (Chichilnisky, 2001; Baccus and Meister, 2002). In particular, we calculated the spatiotemporal filter as the spike-triggered average with the two spatial components X and Y, temporally binned at a resolution of 10 ms and extending 600 ms into the past. For each spatial component, the temporal filter part was subsequently normalized so that the sum of squares equaled unity. Conditional nonlinearities for each spatial component were then obtained as histograms of spike frequencies by selecting stimulus segments for which the other spatial component yielded filtered values around zero in the range of $\pm 0.3 \times$ contrast. To compute the histogram, these segments were separated into 20 bins according to the filtered values of the considered spatial component, so that each bin contained the same number of sampling points.

Filter shapes were analyzed through their time-to-peak, rise time, and biphasic index as explained in the text. Sensitivity was assessed as the maximal value of the conditional nonlinearity over the range spanned by the histogram of the low-contrast condition. Statistical significance of changes in filter shape and in sensitivity was assessed at the population level with Wilcoxon signed-rank tests. For each individual cell, significance was assessed by partitioning the data into eight groups for each contrast condition and performing Wilcoxon rank-sum tests on the obtained sets of measures. A significance criterion of 5% was used in all cases. Details of the data analysis are provided in [Supplemental Experimental Procedures](#).

SUPPLEMENTAL INFORMATION

Supplemental Information includes two figures, Supplemental Text, and Supplemental Experimental Procedures and can be found with this article online at <http://dx.doi.org/10.1016/j.neuron.2012.12.030>.

ACKNOWLEDGMENTS

This work was supported by the Max Planck Society, the German Initiative of Excellence, the International Human Frontier Science Program Organization, and the Deutsche Forschungsgemeinschaft (DFG-SFB 889).

Accepted: December 18, 2012

Published: March 6, 2013

REFERENCES

- Azaredo da Silveira, R., and Roska, B. (2011). Cell types, circuits, computation. *Curr. Opin. Neurobiol.* *21*, 664–671.
- Baccus, S.A., and Meister, M. (2002). Fast and slow contrast adaptation in retinal circuitry. *Neuron* *36*, 909–919.
- Baccus, S.A., Ölveczky, B.P., Manu, M., and Meister, M. (2008). A retinal circuit that computes object motion. *J. Neurosci.* *28*, 6807–6817.
- Beaudoin, D.L., Borghuis, B.G., and Demb, J.B. (2007). Cellular basis for contrast gain control over the receptive field center of mammalian retinal ganglion cells. *J. Neurosci.* *27*, 2636–2645.
- Beaudoin, D.L., Manookin, M.B., and Demb, J.B. (2008). Distinct expressions of contrast gain control in parallel synaptic pathways converging on a retinal ganglion cell. *J. Physiol.* *586*, 5487–5502.
- Berry, M.J., 2nd, Brivanlou, I.H., Jordan, T.A., and Meister, M. (1999). Anticipation of moving stimuli by the retina. *Nature* *398*, 334–338.
- Bölinger, D., and Gollisch, T. (2012). Closed-loop measurements of iso-response stimuli reveal dynamic nonlinear stimulus integration in the retina. *Neuron* *73*, 333–346.
- Bonin, V., Mante, V., and Carandini, M. (2005). The suppressive field of neurons in lateral geniculate nucleus. *J. Neurosci.* *25*, 10844–10856.
- Borst, A., Flanagan, V.L., and Sompolinsky, H. (2005). Adaptation without parameter change: Dynamic gain control in motion detection. *Proc. Natl. Acad. Sci. USA* *102*, 6172–6176.
- Brown, S.P., and Masland, R.H. (2001). Spatial scale and cellular substrate of contrast adaptation by retinal ganglion cells. *Nat. Neurosci.* *4*, 44–51.
- Burkhardt, D.A., Fahey, P.K., and Sikora, M. (1998). Responses of ganglion cells to contrast steps in the light-adapted retina of the tiger salamander. *Vis. Neurosci.* *15*, 219–229.
- Burrone, J., and Lagnado, L. (2000). Synaptic depression and the kinetics of exocytosis in retinal bipolar cells. *J. Neurosci.* *20*, 568–578.
- Chander, D., and Chichilnisky, E.J. (2001). Adaptation to temporal contrast in primate and salamander retina. *J. Neurosci.* *21*, 9904–9916.
- Chichilnisky, E.J. (2001). A simple white noise analysis of neuronal light responses. *Network* *12*, 199–213.
- Dahmen, J.C., Keating, P., Nodal, F.R., Schulz, A.L., and King, A.J. (2010). Adaptation to stimulus statistics in the perception and neural representation of auditory space. *Neuron* *66*, 937–948.
- Dean, I., Harper, N.S., and McAlpine, D. (2005). Neural population coding of sound level adapts to stimulus statistics. *Nat. Neurosci.* *8*, 1684–1689.
- Demb, J.B. (2008). Functional circuitry of visual adaptation in the retina. *J. Physiol.* *586*, 4377–4384.
- Demb, J.B., Haarsma, L., Freed, M.A., and Sterling, P. (1999). Functional circuitry of the retinal ganglion cell's nonlinear receptive field. *J. Neurosci.* *19*, 9756–9767.
- Demb, J.B., Zaghoul, K., Haarsma, L., and Sterling, P. (2001). Bipolar cells contribute to nonlinear spatial summation in the brisk-transient (Y) ganglion cell in mammalian retina. *J. Neurosci.* *21*, 7447–7454.
- Enroth-Cugell, C., and Robson, J.G. (1966). The contrast sensitivity of retinal ganglion cells of the cat. *J. Physiol.* *187*, 517–552.
- Freed, M.A., and Sterling, P. (1988). The ON-alpha ganglion cell of the cat retina and its presynaptic cell types. *J. Neurosci.* *8*, 2303–2320.
- Garcia-Lazaro, J.A., Ho, S.S., Nair, A., and Schnupp, J.W. (2007). Shifting and scaling adaptation to dynamic stimuli in somatosensory cortex. *Eur. J. Neurosci.* *26*, 2359–2368.
- Gaudry, K.S., and Reinagel, P. (2007). Contrast adaptation in a nonadapting LGN model. *J. Neurophysiol.* *98*, 1287–1296.
- Gollisch, T., and Herz, A.V. (2004). Input-driven components of spike-frequency adaptation can be unmasked in vivo. *J. Neurosci.* *24*, 7435–7444.
- Gollisch, T., and Meister, M. (2010). Eye smarter than scientists believed: neural computations in circuits of the retina. *Neuron* *65*, 150–164.
- Hosoya, T., Baccus, S.A., and Meister, M. (2005). Dynamic predictive coding by the retina. *Nature* *436*, 71–77.
- Itti, L., and Koch, C. (2001). Computational modelling of visual attention. *Nat. Rev. Neurosci.* *2*, 194–203.
- Jarsky, T., Cembrowski, M., Logan, S.M., Kath, W.L., Rieke, H., Demb, J.B., and Singer, J.H. (2011). A synaptic mechanism for retinal adaptation to luminance and contrast. *J. Neurosci.* *31*, 11003–11015.
- Kastner, D.B., and Baccus, S.A. (2011). Coordinated dynamic encoding in the retina using opposing forms of plasticity. *Nat. Neurosci.* *14*, 1317–1322.
- Kim, K.J., and Rieke, F. (2001). Temporal contrast adaptation in the input and output signals of salamander retinal ganglion cells. *J. Neurosci.* *21*, 287–299.
- Kim, K.J., and Rieke, F. (2003). Slow Na⁺ inactivation and variance adaptation in salamander retinal ganglion cells. *J. Neurosci.* *23*, 1506–1516.
- Kolb, H., and Nelson, R. (1993). OFF-alpha and OFF-beta ganglion cells in cat retina: II. Neural circuitry as revealed by electron microscopy of HRP stains. *J. Comp. Neurol.* *329*, 85–110.
- Kvale, M.N., and Schreiner, C.E. (2004). Short-term adaptation of auditory receptive fields to dynamic stimuli. *J. Neurophysiol.* *91*, 604–612.
- Li, G.L., Vigh, J., and von Gersdorff, H. (2007). Short-term depression at the reciprocal synapses between a retinal bipolar cell terminal and amacrine cells. *J. Neurosci.* *27*, 7377–7385.
- Maffei, L., Fiorentini, A., and Bisti, S. (1973). Neural correlate of perceptual adaptation to gratings. *Science* *182*, 1036–1038.
- Manookin, M.B., and Demb, J.B. (2006). Presynaptic mechanism for slow contrast adaptation in mammalian retinal ganglion cells. *Neuron* *50*, 453–464.
- Mante, V., Frazor, R.A., Bonin, V., Geisler, W.S., and Carandini, M. (2005). Independence of luminance and contrast in natural scenes and in the early visual system. *Nat. Neurosci.* *8*, 1690–1697.
- Maravall, M., Petersen, R.S., Fairhall, A.L., Arabzadeh, E., and Diamond, M.E. (2007). Shifts in coding properties and maintenance of information transmission during adaptation in barrel cortex. *PLoS Biol.* *5*, e19.
- Movshon, J.A., and Lennie, P. (1979). Pattern-selective adaptation in visual cortical neurones. *Nature* *278*, 850–852.
- Münch, T.A., da Silveira, R.A., Siebert, S., Viney, T.J., Awatramani, G.B., and Roska, B. (2009). Approach sensitivity in the retina processed by a multifunctional neural circuit. *Nat. Neurosci.* *12*, 1308–1316.
- Nagel, K.I., and Doupe, A.J. (2006). Temporal processing and adaptation in the songbird auditory forebrain. *Neuron* *51*, 845–859.
- Ölveczky, B.P., Baccus, S.A., and Meister, M. (2003). Segregation of object and background motion in the retina. *Nature* *423*, 401–408.
- Ölveczky, B.P., Baccus, S.A., and Meister, M. (2007). Retinal adaptation to object motion. *Neuron* *56*, 689–700.
- Ozuysal, Y., and Baccus, S.A. (2012). Linking the computational structure of variance adaptation to biophysical mechanisms. *Neuron* *73*, 1002–1015.
- Rabinowitz, N.C., Willmore, B.D., Schnupp, J.W., and King, A.J. (2011). Contrast gain control in auditory cortex. *Neuron* *70*, 1178–1191.
- Rieke, F. (2001). Temporal contrast adaptation in salamander bipolar cells. *J. Neurosci.* *21*, 9445–9454.

- Samengo, I., and Gollisch, T. (2013). Spike-triggered covariance: geometric proof, symmetry properties, and extension beyond Gaussian stimuli. *J. Comput. Neurosci.* *34*, 137–161.
- Schwartz, G., and Rieke, F. (2011). Perspectives on: information and coding in mammalian sensory physiology: nonlinear spatial encoding by retinal ganglion cells: when $1 + 1 \neq 2$. *J. Gen. Physiol.* *138*, 283–290.
- Schwartz, G.W., Okawa, H., Dunn, F.A., Morgan, J.L., Kerschensteiner, D., Wong, R.O., and Rieke, F. (2012). The spatial structure of a nonlinear receptive field. *Nat. Neurosci.* *15*, 1572–1580.
- Segev, R., Puchalla, J., and Berry, M.J., 2nd. (2006). Functional organization of ganglion cells in the salamander retina. *J. Neurophysiol.* *95*, 2277–2292.
- Shapley, R.M., and Victor, J.D. (1978). The effect of contrast on the transfer properties of cat retinal ganglion cells. *J. Physiol.* *285*, 275–298.
- Shapley, R.M., and Victor, J.D. (1979). Nonlinear spatial summation and the contrast gain control of cat retinal ganglion cells. *J. Physiol.* *290*, 141–161.
- Shapley, R.M., and Victor, J.D. (1981). How the contrast gain control modifies the frequency responses of cat retinal ganglion cells. *J. Physiol.* *318*, 161–179.
- Singer, J.H., and Diamond, J.S. (2006). Vesicle depletion and synaptic depression at a mammalian ribbon synapse. *J. Neurophysiol.* *95*, 3191–3198.
- Smirnakis, S.M., Berry, M.J., Warland, D.K., Bialek, W., and Meister, M. (1997). Adaptation of retinal processing to image contrast and spatial scale. *Nature* *386*, 69–73.
- Solomon, S.G., Peirce, J.W., Dhruv, N.T., and Lennie, P. (2004). Profound contrast adaptation early in the visual pathway. *Neuron* *42*, 155–162.
- Wark, B., Lundstrom, B.N., and Fairhall, A. (2007). Sensory adaptation. *Curr. Opin. Neurobiol.* *17*, 423–429.
- Wark, B., Fairhall, A., and Rieke, F. (2009). Timescales of inference in visual adaptation. *Neuron* *61*, 750–761.
- Weick, M., and Demb, J.B. (2011). Delayed-rectifier K channels contribute to contrast adaptation in mammalian retinal ganglion cells. *Neuron* *71*, 166–179.
- Werblin, F.S. (2010). Six different roles for crossover inhibition in the retina: correcting the nonlinearities of synaptic transmission. *Vis. Neurosci.* *27*, 1–8.
- Wu, S.M., Gao, F., and Maple, B.R. (2000). Functional architecture of synapses in the inner retina: segregation of visual signals by stratification of bipolar cell axon terminals. *J. Neurosci.* *20*, 4462–4470.
- Zaghloul, K.A., Boahen, K., and Demb, J.B. (2005). Contrast adaptation in subthreshold and spiking responses of mammalian Y-type retinal ganglion cells. *J. Neurosci.* *25*, 860–868.
- Zaghloul, K.A., Manookin, M.B., Borghuis, B.G., Boahen, K., and Demb, J.B. (2007). Functional circuitry for peripheral suppression in mammalian Y-type retinal ganglion cells. *J. Neurophysiol.* *97*, 4327–4340.